Acta Crystallographica Section D
Biological Crystallography
ISSN 0907-4449

The structure of *Enterococcus faecalis* thymidylate synthase provides clues about folate bacterial metabolism

Cecilia Pozzi,[a] Stefania Ferrari,[b] Debora Cortesi,[b] Rosaria Luciani,[b] Robert M. Stroud,[c] Alessia Catalano,[d] Maria Paola Costi[b]* and Stefano Mangani[a]*

[a]Dipartimento di Chimica, University of Siena, Via Aldo Moro 2, 53100 Siena, Italy, [b]Dipartimento di Scienze Farmaceutiche, University of Modena and Reggio Emilia, Via Campi 183, 41126 Modena, Italy, [c]Department of Biochemistry and Biophysiscs, University of California, San Francisco, S-412C Genentech Hall, 600 16th Street, San Francisco, CA 94158-2517, USA, and [d]Dipartimento Farmaco-Chimico, University of Bari 'Aldo Moro', Via E. Orabona 4, 70125 Bari, Italy

Correspondence e-mail: mariapaola.costi@unimore.it, stefano.mangani@unisi.it

Received 15 March 2012
Accepted 10 June 2012

PDB Reference: thymidylate synthase, complex with 5-FTHF, 3uwl.

Drug resistance to therapeutic antibiotics poses a challenge to the identification of novel targets and drugs for the treatment of infectious diseases. Infections caused by *Enterococcus faecalis* are a major health problem. Thymidylate synthase (TS) from *E. faecalis* is a potential target for antibacterial therapy. The X-ray crystallographic structure of *E. faecalis* thymidylate synthase (EfTS), which was obtained as a native binary complex composed of EfTS and 5-formyltetrahydrofolate (5-FTHF), has been determined. The structure provides evidence that EfTS is a half-of-the-sites reactive enzyme, as 5-FTHF is bound to two of the four independent subunits present in the crystal asymmetric unit. 5-FTHF is a metabolite of the one-carbon transfer reaction catalysed by 5-formyltetrahydrofolate cyclo-ligase. Kinetic studies show that 5-FTHF is a weak inhibitor of EfTS, suggesting that the EfTS-5–FTHF complex may function as a source of folates and/or may regulate one-carbon metabolism. The structure represents the first example of endogenous 5-FTHF bound to a protein involved in folate metabolism.

1. Introduction

Enterococci are Gram-positive bacteria that exist in a remarkable array of environments. These bacteria can be found in soil, food and water, and they comprise a significant portion of the normal gut flora of humans and animals. Similarly to other bacteria of the gut flora, enterococci also cause infectious diseases. Most clinical isolates are *Enterococcus faecalis* and account for 80–90% of clinical strains. *E. faecium* accounts for the remaining 5–10% of such isolates (Deshpande *et al.*, 2007; Gómez-Gil *et al.*, 2009). Enterococci currently rank fourth in frequency among bacteria isolated from hospitalized patients. Surprisingly, little is known about the factors that contribute to the pathogenicity of enterococci. Some strains of *E. faecalis* and many *E. faecium* strains are resistant to multiple antimicrobials (Deshpande *et al.*, 2007; Teuber *et al.*, 2003). The identification of new antibiotics specifically targeted towards enterococci is of interest and active discovery programs have been initiated to generate novel antibacterial agents. Bacterial thymidylate synthase (TS) represents a validated target for the development of novel antibacterial compounds because bacterial TS inhibitors can discriminate between the bacterial and the host (human) proteins, resulting in low toxicity (Costi *et al.*, 2006). TS (EC 2.1.1.45) catalyses the reductive methylation of 2′-deoxyuridine 5′-monophosphate (dUMP) to 2′-deoxythymidine 5′-monophosphate (dTMP), assisted by the cofactor N^5,N^{10}-methylenetetrahydrofolate (MTHF; see Fig. 1; Carreras &

Santi, 1995; Costi *et al.*, 1999; Stout *et al.*, 1999). TS represents the only synthetic source of dTMP in cells and is a major target for the design of chemotherapeutic agents (Chu *et al.*, 2003).

TS inhibitors, including α156 {3,3-bis(3-chloro-4-hydroxyphenyl)-1*H*,3*H*-benzo[*de*]isochromen-1-one}, have been proposed as antibacterial agents against vancomycin-resistant Gram-positive *Staphylococcus aureus* infections with low toxicity towards human cells. Some of these antimicrobials were also able to inhibit *E. faecalis* clinical isolates (Finer-Moore *et al.*, 2005; Stout *et al.*, 1999). In the current work, we focused on bacterial TS enzymes as novel therapeutic targets and used a structure-determination programme based on the bacterial TS enzymes.

This work presents the first X-ray crystal structure of the *E. faecalis* TS enzyme (EfTS) and the first example of a naturally occurring complex of 5-FTHF with a protein involved in folate metabolism. The structure of the EfTS–5-FTHF complex may serve as a basis for further structure-based design studies aimed at the identification of new antibacterial agents against *E. faecalis* infections.

2. Experimental procedures

2.1. Chemistry

All of the chemicals were purchased from Sigma–Aldrich or Lancaster and were of the highest commercially available quality. All of the solvents were reagent grade.

2.2. Protein cloning, expression and purification

Thymidylate synthase was amplified from *E. faecalis* genomic DNA, cloned into pET-28b (His tag at the amino-terminus) and pET-30a (no His tag) vectors and used to transform DH5α maximum-efficiency cells. The following

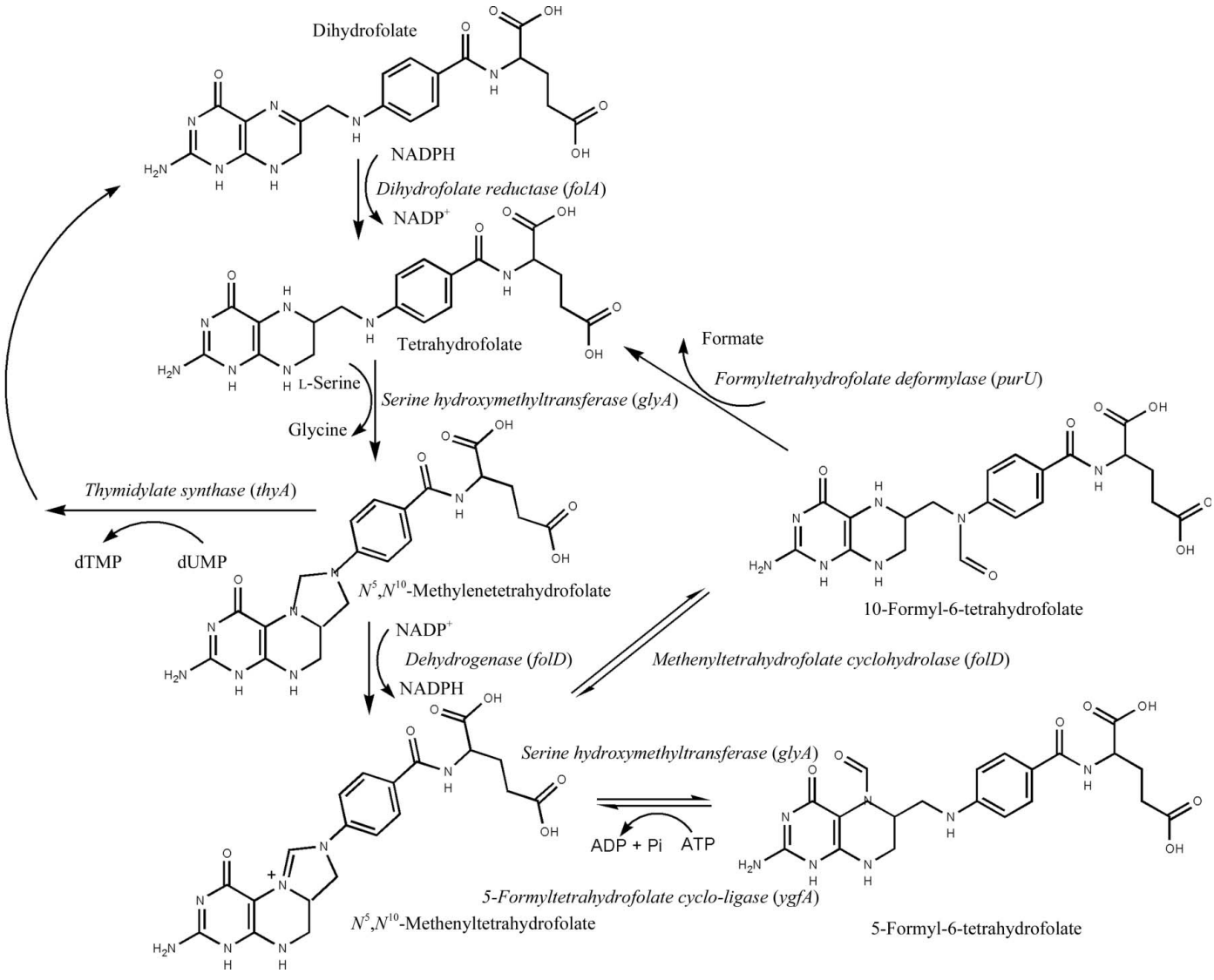

Figure 1
Major folate-dependent pathways in bacterial one-carbon metabolism. The scheme gives the names of the enzymes involved (in italics). The gene names of the enzymes for *E. coli* are given in parentheses. The chemical formulae and the names of the substrates and the products of the reactions are also indicated.

Table 1
Kinetic parameters for EfTS.

	EfTS–5-FTHF complex	EfTS	hTS
K_m, dUMP (μM)	13 ± 2	7 ± 1	10 ± 2
K_m, MTHF (μM)	35 ± 5	20 ± 2	5 ± 1
SA (EU mg^{-1})	1.22 ± 0.50	1.33 ± 0.80	1 ± 0.2
k_{cat} (s^{-1})	2.5 ± 0.5	4.3 ± 0.5	1 ± 0.2
k_{cat}/K_m, dUMP (μM^{-1} s^{-1})	0.20 ± 0.07	0.65 ± 0.15	0.1 ± 0.02
k_{cat}/K_m, MTHF (μM^{-1} s^{-1})	0.07 ± 0.02	0.22 ± 0.04	0.2 ± 0.04
K_i, 5-FTHF (μM)		208 ± 15	

primers were used: the 5′ primer 5′-CGGAGGGAATCATATGGAAG and the 3′ primer 5′-GCTTCTCTCTCGAGTTTTATACGG. The DNA sequence of the inserted gene was confirmed (UCSF Genomic Core Facilities). The EfTS gene in the pET-28b vector (designated pEfTS-His) and in the pET30b vector (designated pEfTS) was expressed in *Escherichia coli* BL21 (DE3) cells. The untagged protein was purified and used for further studies.

Protein purification was performed following the protocol used for *E. coli* thymidylate synthase (EcTS) with minor modifications (Maley & Maley, 1988). The bacterial strain was cultured in 2 l LB medium containing 50 µg ml^{-1} kanamycin at 310 K with shaking at 120 rev min^{-1}. Expression of thymidylate synthase was induced to an absorbance of 0.6 at 600 nm with 1 m*M* isopropyl β-D-1-thiogalactopyranoside (IPTG). Induction lasted for 4 h at 310 K.

The cells were centrifuged at 4000 rev min^{-1} for 30 min at 277 K. The cell pellets were frozen until further use. A cell pellet was suspended in 16 ml 25 m*M* KH_2PO_4/K_2HPO_4 pH 7.5, 7.0 m*M* EDTA (buffer *A*) containing Complete protease inhibitor and sonicated. The broken cells were centrifuged for 40 min at 12 000 rev min^{-1} at 277 K and the pellet was discarded. All purification steps were conducted at 277 K. The supernatant was treated with 10% streptomycin, stirred for 10 min and centrifuged for 30 min at 12 000 rev min^{-1} and 277 K. The supernatant was loaded onto a DEAE-Sephacel column. The enzyme was eluted with a 30–60% gradient from buffer *A* to a buffer consisting of 50 m*M* KH_2PO_4/K_2HPO_4 pH 6.5, 20 m*M* β-mercaptoethanol, 1 *M* NaCl. Solid ammonium sulfate was added to the pooled DEAE fractions to a final concentration of 1 *M* and the mixture was loaded onto a Phenyl Sepharose 6 Fast Flow column pre-equilibrated with buffer *B* (50 m*M* KH_2PO_4/K_2HPO_4 pH 6.5, 4 *M* ammonium sulfate, 1 m*M* EDTA, 20 m*M* β-mercaptoethanol). The enzyme was eluted with a 0–100% gradient from buffer *B* to a buffer consisting of 50 m*M* KH_2PO_4/K_2HPO_4 pH 6.5, 0.5 *M* ammonium sulfate, 1 m*M* EDTA, 20 m*M* β-mercaptoethanol. The pooled fractions were then dialysed in 25 m*M* KH_2PO_4/K_2HPO_4 buffer pH 7.5 for 10 h and stored at 193 K.

2.3. Enzymology

The enzyme-kinetics experiments were conducted using a chromogenic assay under standard conditions (Pogolotti *et al.*, 1986). The kinetic parameters reported for EfTS and human thymidylate synthase (hTS) are the mean of triplicate measurements (Table 1).

The inhibition patterns of the compounds were determined by steady-state kinetic analysis of the dependence of enzyme activity on MTHF concentration at varying inhibitor concentrations. All of the compounds showed competitive inhibition with respect to MTHF. The apparent inhibition constants ($K_{i,app}$, referred to as K_i in the text) were obtained from linear least-squares fits of the residual activity as a function of inhibitor concentration using suitable equations for competitive inhibition (Segel, 1975). The reaction mixture was the same for the inhibition assay and the TS standard assay. Stock solutions of each inhibitor were freshly prepared in dimethyl sulfoxide (DMSO) and stored at 193 K. The concentration of DMSO in the reaction mixture did not exceed 5%.

2.4. Crystallization

Crystallization trials for EfTS were performed using the sitting-drop vapour-diffusion method (Benvenuti & Mangani, 2007) at 297 K. Crystal Screen, Crystal Screen 2 and Grid Screen Ammonium Sulfate from Hampton Research were used for screening crystallization conditions. Drops consisting of 2 µl precipitant solution and 1 µl EfTS solution (7.8 mg ml^{-1} in 25 m*M* KH_2PO_4/K_2HPO_4 pH 6.8, 40 m*M* dUMP, 1 m*M* EDTA) were equilibrated against 100 µl reservoir solution. After one month, crystals were observed in a drop containing 3.2 *M* ammonium sulfate, 0.1 *M* HEPES buffer pH 7.0 as the precipitant solution. These crystals were ill-formed and provided a poor diffraction pattern when exposed to X-ray radiation. Therefore, we attempted to improve the crystal ordering/quality by applying seeding techniques (Benvenuti & Mangani, 2007). The obtained crystals were crushed and seeding solutions were prepared by dilution with the successful precipitant solution (3.2 *M* ammonium sulfate, 0.1 *M* HEPES buffer pH 7.0). Drops (4 µl) of a 2.5 mg ml^{-1} EfTS solution in 25 m*M* KH_2PO_4/K_2HPO_4 pH 6.8, 40 m*M* dUMP, 1 m*M* EDTA were mixed with 2 µl of a precipitant solution consisting of 2.7 *M* ammonium sulfate, 0.1 *M* HEPES buffer pH 7.0. Streak-seeding was performed at different dilutions of the seeding solution. The drops were allowed to equilibrate at room temperature over 0.6 ml precipitant-solution wells. Crystals suitable for diffraction appeared within 2–3 weeks in drops to which seeding solution (diluted 1:100) had been applied. Before data collection, the crystals were transferred into a cryoprotectant solution consisting of 20% ethylene glycol and 80% precipitant solution (2.7 *M* ammonium sulfate, 0.1 *M* HEPES pH 7.0) and flash-cooled in liquid nitrogen.

2.5. Structure solution and refinement

The EfTS data were collected on ESRF (European Synchrotron Radiation Facility) beamline ID23-2. A complete data set was recorded from a single cooled crystal using 0.5° oscillation images. The intensities were integrated using *MOSFLM* (Leslie, 2006) and scaled with *SCALA* (Evans, 2006) from the *CCP*4 suite (Winn *et al.*, 2011). The data-collection statistics are reported in Table 2. The crystals

Table 2
Data-collection and refinement statistics.

Values in parentheses are for the highest resolution shell.

PDB code	3uwl
X-ray source	ID23-2, ESRF, Grenoble, France
Wavelength (Å)	0.8726
Data-collection temperature (K)	100
Space group	$P2_1$
Unit-cell parameters (Å, °)	a = 71.94, b = 94.25, c = 96.19, β = 95.01
Subunits in asymmetric unit	4
Matthews coefficient (Å^3 Da^{-1})	2.28
Solvent content (%)	46.19
Data-reduction statistics	
Resolution limits (Å)	33.60–2.07 (2.18–2.07)
Reflections measured	237374 (33391)
Unique reflections	75045 (10816)
Completeness (%)	96.3 (95.2)
R_{merge} (%)	11.7 (39.3)
Multiplicity	3.2 (3.1)
$\langle I/\sigma(I)\rangle$	8.8 (3.2)
Wilson B factor (Å^2)	14.0
Refinement statistics	
Resolution range (Å)	33.49–2.07 (2.12–2.07)
Reflections used	71263
R_{cryst} (%)	16.0 (18.7)
R_{free} (%)	21.7 (24.7)
R_{free} test-set size	3757
Total atoms (protein/ligand/water) in refinement	10761
Protein atoms	9832
5-FTHF atoms	68
Ethylene glycol molecules	32
Sulfate ions	30
Water molecules	799
Refinement type	Restrained refinement with TLS parametrization
Average B factor (Å^2)	9.61
R.m.s. deviation from ideal	
Bond lengths (Å)	0.015
Bond angles (°)	1.495
Planar groups (Å)	0.007
Chiral centres (Å^3)	0.118
E.s.d. on atomic positions from ML refinement (Å)	0.114
Ramachandran plot (%)	
Most favoured	91.9
Allowed	8.1
Disallowed	0.0

belonged to space group $P2_1$, with four independent EfTS subunits in the asymmetric unit.

The EfTS structure was solved by the molecular-replacement technique as implemented in *MOLREP* (Vagin & Teplyakov, 2010) from the *CCP*4 suite using the crystal structure of *Lactobacillus casei* TS (LcTS) as a model (PDB entry 2tdm; 73% sequence homology; Finer-Moore *et al.*, 1993).

Because of the structural flexibility that characterizes several domains of the TS enzymes, the LcTS loop 82–144 was removed from the model. *MOLREP* provided the correct solution, which consisted of EfTS homodimers (*AB* and *CD*) in the crystal asymmetric unit.

The EfTS molecule was manually rebuilt in the electron-density maps. The entire polypeptide chain could be reconstructed in only one subunit of each dimer (subunits *B* and *D*), as the regions corresponding to residues 98–118 of the *A* subunit and residues 92–122 of the *C* subunit were not clearly visible in the electron-density maps. The final model was refined using *REFMAC*5 (Murshudov *et al.*, 2011) from the *CCP*4 suite using TLS parameterization (Winn *et al.*, 2001). The optimal partitioning of the EfTS polypeptide was obtained through the *TLS Motion Determination* web server (Painter & Merritt, 2006*a*,*b*). Each of the four enzyme subunits present in the asymmetric unit was partitioned into six continuous TLS segments. The resulting TLS parameterization was included in the final cycles of the refinement protocol.

Between the refinement cycles, the model was subjected to manual rebuilding using *Coot* (Emsley & Cowtan, 2004). Upon completion of the protein model, inspection of the Fourier difference map clearly demonstrated the presence of a ligand bound to the active sites of subunits *B* and *D*. The map indicated that the ligand was a derivative of tetrahydrofolate modified at position 5 of the pteridine ring. The molecule was modelled and refined as either 5-formyl-6-tetrahydrofolate (5-FTHF) or 5-hydroxymethyl-6-tetrahydrofolate (5-HMTHF). Tetrahedral anions from the crystallization buffer (most likely to be sulfate anions owing to the much higher concentration present in the crystallization solution) were found to be bound to all subunits. Six molecules were included in the model and refined as sulfates. The final model also included 799 water molecules that were added using *ARP*/*wARP* (Morris *et al.*, 2003) and eight ethylene glycol molecules from the cryoprotectant solution. The stereochemical quality of the final model was checked using *PROCHECK* (Laskowski *et al.*, 1993). The structural models were rendered using *CCP*4*mg* (Potterton *et al.*, 2002). Refinement statistics are reported in Table 2.

3. Results

3.1. Crystal structure

The crystal structure of the 'as-prepared' EfTS (EC 2.1.1.45) shows the constitutive dimeric quaternary structure of the enzyme which is present in solution as indicated by gel-filtration chromatography (data not shown). The homodimeric quaternary structure of EfTS is characteristic of all of the characterized TS enzymes (Finer-Moore *et al.*, 1994; Fox *et al.*, 1999; Hardy *et al.*, 1987; Perry *et al.*, 1990; Schiffer *et al.*, 1995). The TSs of different organisms share the same overall tertiary and quaternary structure despite having variable levels of sequence homology ranging from 35 to 70% identical residues (*e.g.* 47% identity between hTS and EfTS). A sequence comparison of EfTS with other bacterial and eukaryotic TS enzymes of known structure is shown in Fig. 2. The alignment shows that the TS enzymes from the Gram-positive bacteria *Bacillus subtilis* and *L. casei* share 34 and 73% sequence homology, respectively, with EfTS.

In the EfTS crystal, two independent dimers are present in the asymmetric unit and are related by an almost exact noncrystallographic twofold axis close to the cell *a* axis. Although the two dimers have essentially identical structures, each dimer is asymmetric, as shown in Fig. 3(*a*). Each of the

two EfTS dimers (subunits *AB* and *CD*) shows subunit heterogeneity owing to the presence of a ligand bound in the active-site cavity of one subunit in each dimer (subunits *B* and *D*). Ligand binding modifies the conformation and mobility of a domain that covers the active-site cavity (see below), resulting in different conformations of the EfTS subunits involved in the dimer.

A cartoon representation of the EfTS quaternary and tertiary structures is shown in Figs. 3(*a*) and 3(*b*). Each subunit of the enzyme is composed of two domains. The larger domain (residues 1–68 and 139–315) has an α/β structure characterized by seven α-helices and eight β-strands. This domain represents the conserved core of the enzyme. The small domain (residues 69–138) is structured and fully visible in the electron-density maps only for the ligand-bound subunits *B* and *D* (see below), in which it covers the active-site cavity. The fold of the small domain, as seen in the complete *B* and *D* subunits, is characterized by five α-helices connected by loops.

In the *A* and *C* subunits of EfTS the small domain is partially ordered and only three helices of the *A* and *C* subunits and part of a loop (residues 91–97 in subunit *A*) could be modelled into the electron density.

The EfTS dimer interface is principally formed by extensive contacts among the side chains of the residues from the five-stranded β-sheet present in the large domain of each subunit. The remaining portion of the interface is composed of residues from the interconnecting loops. 47 residues from each subunit contribute to the interface, of which 16 are completely solvent-inaccessible. The program *PISA* (http://www.ebi.ac.uk/msd-srv/prot_int/pistart.html; Krissinel & Henrick, 2007) was used to analyse the dimer interfaces. The total buried surface area at the interface (2244 Å^2 for the *AB* dimer and 2259 Å^2 for the *CD* dimer) agrees with the dimeric quaternary structure of EfTS that is maintained in solution (Fig. 3*a*). Many hydrophilic interactions occur between the monomers. An average of 34 potential hydrogen bonds and nine potential salt bridges were identified across the interface.

Superimposition of the crystal structures of different TSs from eukaryotic and prokaryotic sources highlights the presence of a highly conserved α/β-core structure that represents the

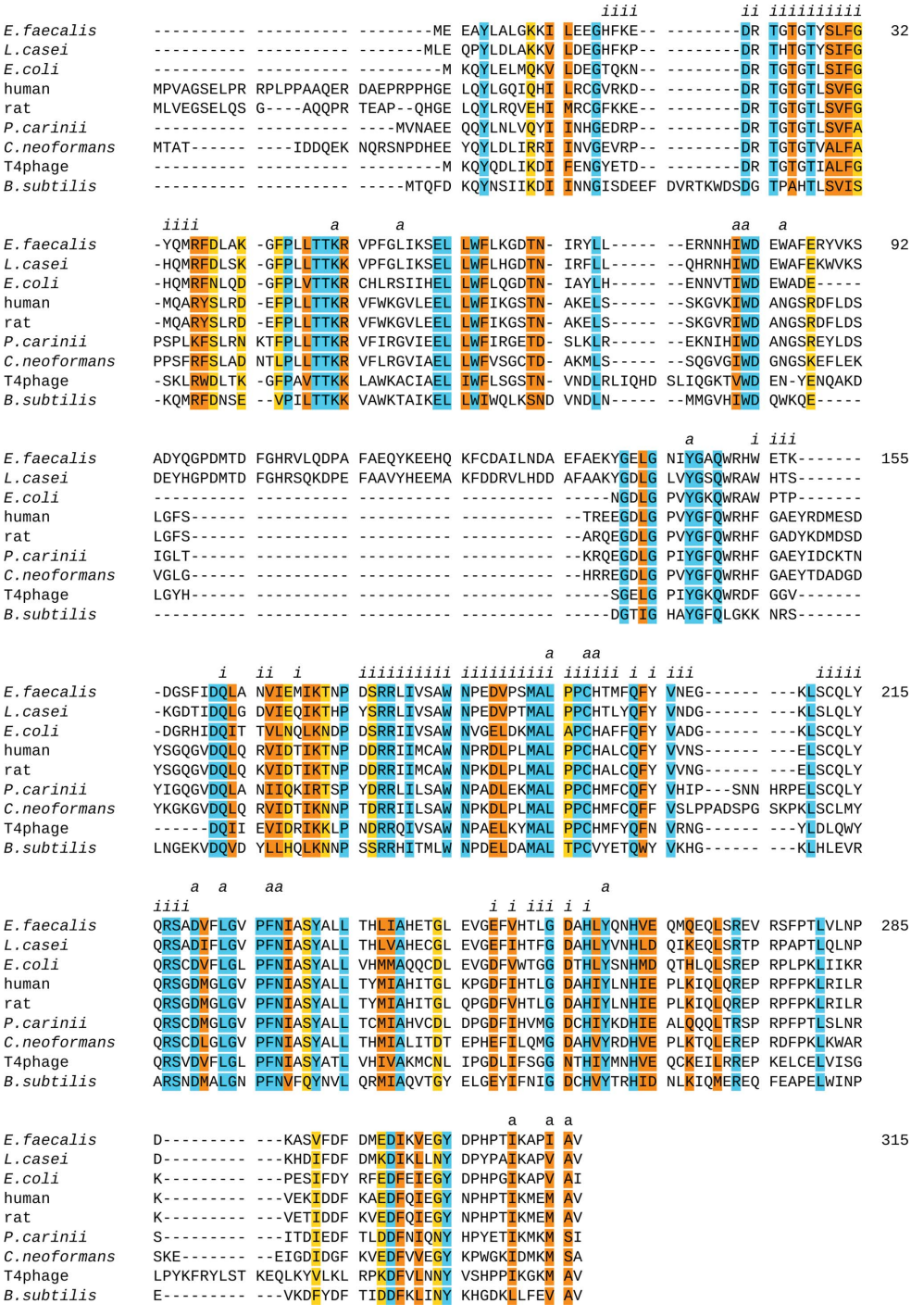

Figure 2
Sequence alignment among nine different species. Identical residues are highlighted in cyan, residues with conservative changes are highlighted in orange and residues with similar changes are highlighted in yellow. Residues located at the monomer–monomer interface of the EfTS enzyme are marked by an italic letter *i*, while active-site residues are marked by an italic letter *a*.

majority of the large domain of TS enzymes (Fig. 4*a*). Among the TSs for which structures have been determined, human TS is unique in that the catalytic core of the apoenzyme can also adopt an inactive conformation. In this inactive conformation the loop containing the catalytic cysteine is refolded, thereby orienting the catalytic sulfhydryl towards the dimer interface. Ligand binding stabilizes the active form of the enzyme in which the catalytic loop is shifted and the catalytic Cys195 is exposed to the active site (Berger *et al.*, 2004). The mobility of the catalytic loop is characteristic of the human enzyme and is larger than that observed in EfTS.

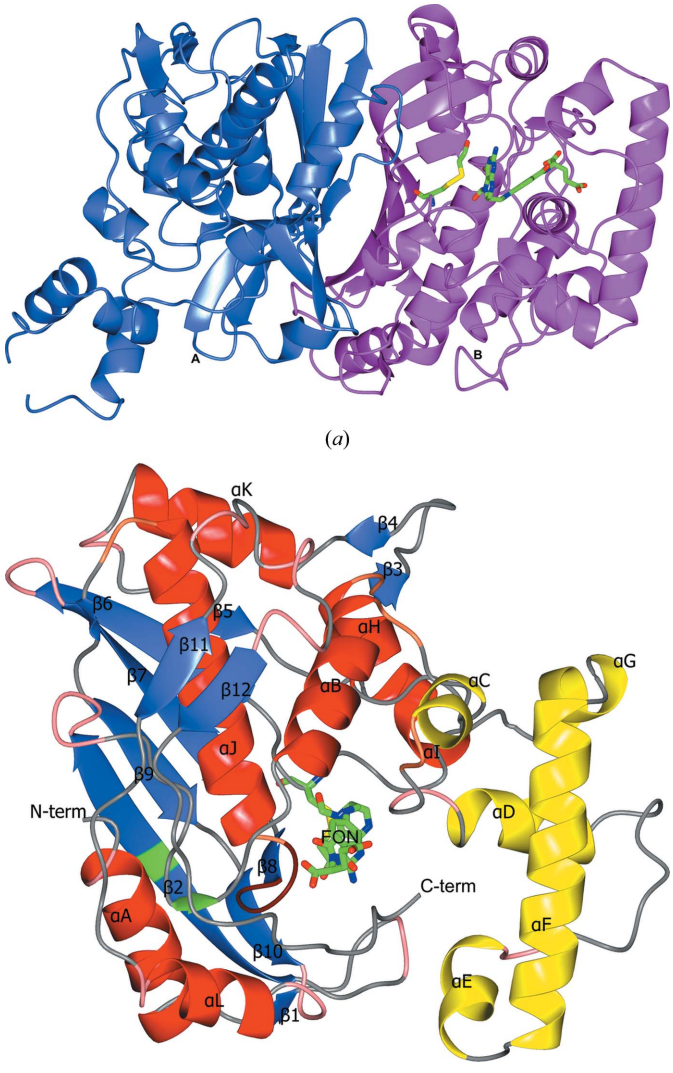

Figure 3
(*a*) Quaternary structure of EfTS. The two subunits of the heterodimer differ in the conformation of the small domain owing to the presence of a ligand bound to one of the active-site cavities. The ligand-bound subunit (magenta) is in a closed conformation, while the unbound subunit (light blue) is in an open conformation. The ligand is represented as sticks in CPK colours. (*b*) Cartoon representation of the tertiary fold of the EfTS *B* subunit with secondary structure labelled. The small domain is yellow, while the large domain has β-strands coloured light blue and α-helices coloured red. Unstructured loops are in grey, type 3 turns are in pink, type 4 turns are in tan, type 5 turns are in coral and β-bulges are in green, as is the location of the S–S bridge.

Large differences are found in the small domain (Fig. 4*b*). Although the small domain of EfTS is very similar to that presented by *L. casei* TS (Hardy *et al.*, 1987), this domain is absent in *E. coli* TS (Perry *et al.*, 1990). The two parts of the conserved core are connected through a loop composed of five amino acids (residues 84–89 in EcTS). In the crystal structures of the human enzyme (Schiffer *et al.*, 1995) this domain is completely visible for the ternary complexes and contains the substrate and cofactor or their analogues (Berger *et al.*, 2004).

The active site of the EfTS enzyme is a shallow cavity embedded between the two domains (Fig. 3*b*). A wall of this cavity is formed by the β-turn between strands 7 and 8, by the loop between β7 and αN and by the first part of the same helix. The opposite wall is formed by the loop between β-strands 1

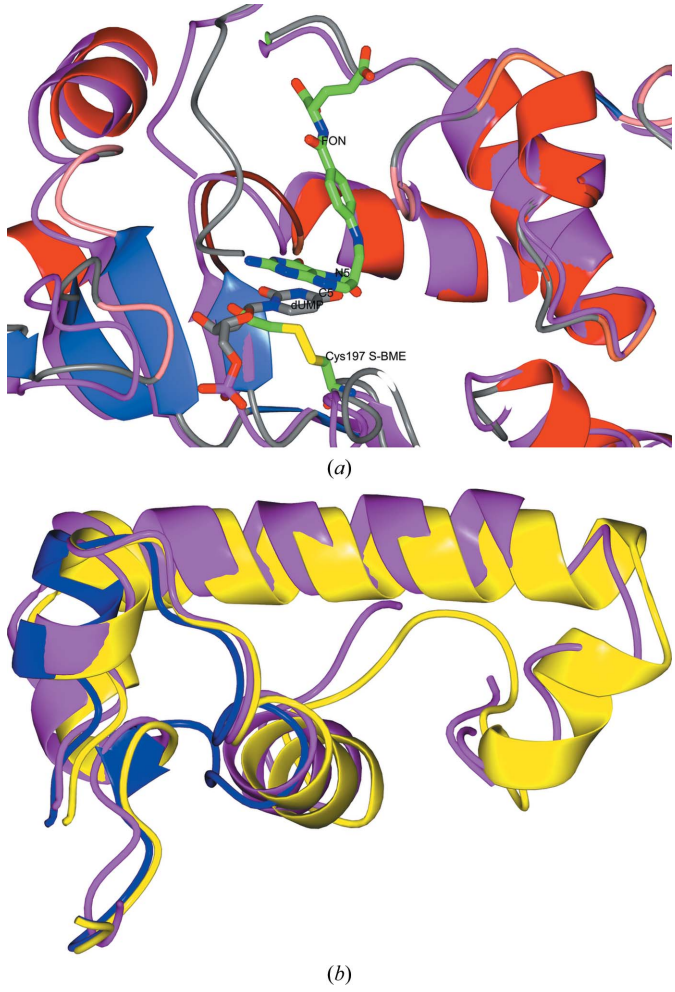

Figure 4
(*a*) Least-squares superimposition of the large domain of the EfTS–5-FTHF complex (light-blue β-strands and red α-helices) with the analogous domain of the binary complex LcTS–dUMP (magenta; unpublished data from our laboratory). The similarity of the structures of the two enzymes can be appreciated as well as the occlusion of the dUMP-binding site by the chemical modification of EfTS Cys197. (*b*) Least-squares superimposition of the small domain of the EfTS–5-FTHF complex (yellow) with the analogous domain of the binary complex LcTS–dUMP (magenta; unpublished data from our laboratory) and the small domain of EcTS (blue; unpublished data from our laboratory). The similarity of the EfTS and LcTS small domains contrasts with the completely different structure of the small domain of EcTS.

and 2. The catalytic residue Cys197 is located on the loop between αM and β6. This wall is completed by several residues on the loop between αL and β5 of the facing subunit. In particular, two residues (Arg177 and Arg178) protrude directly into the cavity, as observed in other TS enzymes. The cavity is completed by the C-terminal segment, which only becomes ordered and fully visible in the ligand-bound subunit. The ordering is a consequence of the noncovalent interactions (hydrophobic and hydrogen bonds) that link 5-FTHF to the Ala314 backbone carbonyl and to the Ile313 side chain (Fig. 5). Interestingly, the above interactions cause a movement by approximately 7.5 Å of the loop linking strands β1 and β2 (Lys19–Thr27), which is stabilized in this conformation by a salt link between Arg22 and the carboxylate terminus (Val315).

When the small domain is in the 'closed' conformation, helices αD and αE cover the active site.

The dimer subunits differ in terms of the conformation and the active-site composition. Additional electron density belonging to an exogenous ligand is present in the active sites of subunits *B* and *D* only, in which a large positive electron density is visible in the Fourier difference maps (Fig. 5). Such additional electron density is consistent with a folate-like molecule. Refinement demonstrated that the ligand could be either (6*S*)-5-hydroxymethyl-6-tetrahydrofolate (5-HMTHF) or (6*S*)-5-formyl-6-tetrahydrofolate (5-FTHF) because the pyrazine ring of the folate pteridine moiety was in a puckered conformation (*i.e.* in the reduced form). The chain present at pteridine C5 revealed the presence of two atoms that are consistent with either a CH_2-OH or a CH=O group (5-CH_2-CH_3 tetrahydrofolate is not known). The ligand could be refined as either 5-FTHF or 5-HMTHF without significant changes in either the refinement quality indicators or the resulting Fourier difference maps, as expected. At the resolution of the present structure (2.07 Å), single and double C—O bonds cannot be distinguished (Figs. 1 and 5). However, we opted for the 5-formyl derivative (5-FTHF) because this compound naturally occurs in the cell (Stover & Schirch, 1993) and in both subunits the 5-FTHF formyl O atom is not engaged in hydrogen bonds to the O4 atom of the pteridine ring, as would be expected if the enol form (5-HMTHF) was present. Such enol–keto tautomeric equilibrium of 5-FTHF has previously been observed in the crystal structure of the complex between *E. coli* dihydrofolate reductase and 5-FTHF (Lee *et al.*, 1996).

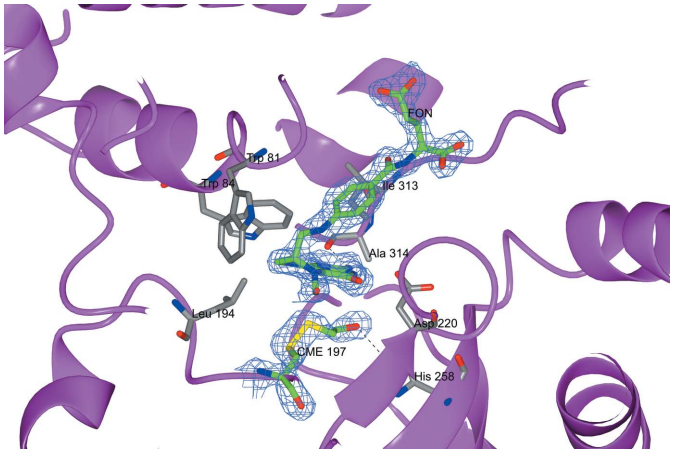

Figure 5
Stick representation of the 5-FTHF ligand bound to the *B* and *D* subunits of EfTS with superimposed electron-density map (blue wire at 1.5σ) computed with $2F_o - F_c$ coefficients and refined phases. The β-mercaptoethanol-modified Cys197 is also shown as sticks, together with other relevant residues in the active-site cavity.

Although the crystals were grown in the presence of dUMP, no binding of this substrate was detected in any subunit. This effect may arise from competition for the same binding site of dUMP with the sulfate used at high concentration in the crystallization of EfTS. However, in several other instances dUMP binding has been observed under similar crystallization conditions (Sage *et al.*, 1996; Birdsall *et al.*, 2003; Mangani *et al.*, 2011). We also attempted to obtain crystals of ligand-free protein by using extensively dialysed enzyme and microseeding and macroseeding techniques. However, microcrystalline aggregates that were unsuitable for structure determination persisted.

5-FTHF showed the same binding mode in both subunits *B* and *D*. It occupies a large portion of the active-site cavity that spans from the proximity of the catalytic Cys197 towards the opening located between the small domain helix D and the large domain β8 strand, the C-terminus and helices B and J (Fig. 3*b*). This binding site is opposite the dUMP phosphate-binding site occupied in EfTS by a sulfate anion from the crystallization solution. Superposition of the EfTS–5-FTHF complex with LcTS–dUMP (Fig. 4*a*) clearly shows the different binding sites for the two molecules, which taken together are close to those presumably adopted by the productive ternary complex MTHF–dUMP, as the 5-FTHF N5 atom, which mimics the reactive N5 atom of MTHF, and the dUMP C5 atom are very close and optimally oriented for reaction.

5-FTHF is within contact distance of the catalytic Cys197, which is in the form of *S*,*S*-(2-hydroxyethyl)thiocysteine (CME) only in the subunits in which 5-FTHF is bound and was obtained by reaction with β-mercaptoethanol (βME) in the protein buffer. Modification of the active-site cysteine presumably prevents binding of dUMP and provides a binding surface for the pteridine ring of the folate, as dUMP does in ternary complexes of TS. Several other hydrophobic interactions occur between 5-FTHF and residues Leu55, Trp81, Leu194 and Phe227. Three hydrogen bonds are established between 5-FTHF and the Asp220 and Asn228 side chains and the Ala314 carbonyl O atom. All of the other hydrogren bonds are between 5-FTHF and water molecules. The binding mode and conformation of 5-FTHF observed here is very similar to that observed for folate in the structures of *E. coli* (Hyatt *et al.*, 1997) and *B. subtilis* (Fox *et al.*, 1999) TS ternary complexes with 5-fluoro-2′-deoxyuridine 5′-monophosphate (FdUMP). However, in EfTS the binding occurs without the presence of a dUMP analogue, the position of which is occupied by the hydroxyethyl moiety of the modified Cys197 (Figs. 4*a* and 5). The side chain of CME makes the same interactions in both

the *B* and *D* subunits: the SG atom of CME is within contact distance of the NH2 group of Arg217, while the SD atom makes contacts with the pteridine rings of 5-FTHF. Finally, the terminal hydroxyl group of CME is involved in two hydrogen bonds to His258 $N^{\epsilon 2}$ and Tyr260 OH. A total of six sulfate anions from the crystallization solution are found bound to the EfTS dimers. Four sulfates, one in each subunit and independently of the binding of 5-FTHF to the active site, occupy the usual binding site of the dUMP phosphate group constituted by Arg217 of one subunit and Arg177 and Arg178 of the facing subunit of the dimer. In the subunits in which 5-FTHF is bound, Arg22 also binds to sulfate. The remaining two sulfate anions are bound only in subunits in which 5-FTHF is bound and form salt links with Arg50 (loop β2–αB) and Thr308 from the C-terminus.

3.2. EfTS kinetics and ligand binding

5-FTHF cocrystallizes with EfTS; therefore, it is present during the entire purification process. To study the kinetic properties of native EfTS, the enzyme was dialyzed to obtain the kinetically characterized apoenzyme together with the 5-FTHF-bound form of the enzyme. Table 1 shows the kinetic data for both native and 5-FTHF-bound enzyme compared with those of human thymidylate synthase (hTS).

The K_m values for dUMP and methylenetetrahydrofolate (MTHF) are higher for 5-FTHF–EfTS than for the apoenzyme. This difference is a consequence of the active site being partially occupied by a weak inhibitor (5-FTHF), which reduces the efficacy of the interaction of the substrates with the protein. The k_{cat} values show the same trend, with the k_{cat} value for the complexed enzyme being smaller than the k_{cat} for the native enzyme. The specificity of the enzyme, given by k_{cat}/K_m, is also higher for the native enzyme than for the complexed enzyme.

5-FTHF was tested for inhibition of native EfTS, giving a K_i of 208 $\pm$ 15 μM. The effect of the 5-FTHF concentration on the enzyme activity was studied using variable concentrations of the MTHF substrate and a mixed-type inhibition pattern was found (data not shown). This behaviour can be explained by the observed enzyme conformational change occurring upon binding of 5-FTHF. The conformational change of the small domain causing an alteration of the binding sites for dUMP and the cofactor affects the binding of both substrates. Overall, the kinetic data indicate that the 5-FTHF-complexed enzyme has lower activity compared with the native enzyme. Considering that 5-FTHF is always present in the cells and that it is a normal metabolite within the folate pathways, our results suggest that 5-FTHF may function as a negative modulator of EfTS depending on the cellular concentration of this ligand. However, alternative explanations for the presence of 5-FTHF in the enzyme active site are possible (see §4).

4. Discussion

The biochemical and kinetic data from several TS species indicate that TS is an enzyme with half-of-the-sites reactivity and that substrates bind more strongly to one active site than the other (Carreras & Santi, 1995; Maley *et al.*, 1995; Spencer *et al.*, 1997; Gibson *et al.*, 2008, 2011). Nearly all of the TS structures determined to date, including both binary and ternary complexes, are comprised of symmetric dimers and provide little insight into the basis of this negative cooperativity. The EfTS structure determined in this work is the second structure in which substrates or substrate analogues are bound asymmetrically to the TS dimer. The other example is the TS enzyme from the fungus *Pneumocystis carinii* (Anderson *et al.*, 1999). This result provides strong evidence that *E. faecalis* TS is an enzyme with half-of-the-sites reactivity. The subunits at which the 5-FTHF molecules are bound are inhibited by this compound, thereby demonstrating Michaelis–Menten mixed-type inhibition with a K_i of 208 μM. The observed X-ray structure accounts for these data. The binding mode observed for 5-FTHF provides a natural scaffold for the design of more potent inhibitors directed against EfTS, as has been performed for other TS enzymes (*i.e.* bacterial and human TS; Mangani *et al.*, 2011). Specifically inhibiting the bacterial enzyme with respect to the human enzyme may be possible based on structural comparison between EfTS and hTS, with a focus on two features. Firstly, EfTS has a more extended small domain and lacks the eukaryote-specific eight-residue insertion (residues 102–109) that is present in hTS. Secondly, the structural flexibility of the two enzymes is different and leaves different binding sites accessible to the interacting ligands. This aspect has been observed previously in other TS enzymes such as EcTS and PcTS, in which differential inhibition was observed with respect to hTS (Ferrari *et al.*, 2003). The differential inhibition arose from the different flexibilities of the pathogenic enzymes with respect to hTS. No data exist on these aspects, but we have recently demonstrated that it is possible to specifically inhibit the EfTS recombinant protein with respect to the human enzyme (hTS; Mangani *et al.*, 2011; Ferrari *et al.*, 2003).

The binding of folate-like molecules and analogues to TS and dihydrofolate reductase (DHFR) enzymes has previously been observed in several instances, including in the ternary complexes of *E. coli* TS with FdUMP and C_2H_4-folate or its analogue 10-propargyl-5,8-dideazafolate (CB3717) (Matthews, Appelt *et al.*, 1990; Matthews, Villafranca *et al.*, 1990; Perry *et al.*, 1993) and in the ternary complex of *P. carinii* TS with dUMP and CB3717 (Anderson *et al.*, 1999), in which half-of-the-sites reactivity of TS has been described. Another example is provided by the structure of the ternary complex between *B. subtilis* TS, FdUMP and C_2H_4-folate (Fox *et al.*, 1999). In the case of the catalytically inactive C-terminal deletion mutant of *E. coli* TS, a modified form of 5,10-methylenetetrahydrofolate (Perry *et al.*, 1993) has been interpreted as 5-CH_2-OH-folate. This molecule is a product of hydration of the cofactor 5-iminium ion intermediate rather than 5-FTHF based on the interaction of the ligand with the active-site residues. Negative cooperativity of folinic acid binding to DHFR has also been described (Birdsall *et al.*, 1981; Lee *et al.*, 1996). In all of the above cases, a folate-like molecule has been observed to form a ternary complex: dUMP–

folate–TS. However, in the present structure EfTS appears to be able to bind only 5-FTHF in the active site and not dUMP. This binding behaviour occurs despite the presence of dUMP in the crystallization medium at concentrations that are conducive to the formation of complexes with other bacterial TSs, such as *E. coli* TS and *L. casei* TS (data from our laboratory; Mangani *et al.*, 2011). This behaviour of EfTS can be rationalized if we consider that 5-FTHF occupies the EfTS cavity and is not released during the purification steps and that the 5-FTHF-binding site in part overlaps with the dUMP-binding site, as demonstrated by the higher K_m of dUMP towards the complexed enzyme and by the kinetic profile, in which the ligand shows a mixed-type inhibition pattern *versus* both substrates (Table 1). Moreover, the complex EfTS–5-FTHF undergoes a conformational change (shift of EfTS to an active conformation) that accounts for the limited accessibility to the dUMP-binding site, which is further restricted once the hydroxyethyl-cysteine derivative is formed. All of these factors make the normal binding of dUMP difficult (Fig. 4*a*). Our structure represents the first example of endogenous 5-FTHF bound to a protein involved in folate metabolism. All other reported 5-FTHF complexes have been obtained by adding 5-FTHF to the crystallization solution. 5-FTHF is present in bacterial cell metabolism, where it is formed by the activity of serine hydroxymethyltransferase on 5,10-methenyltetrahydrofolate. The latter compound is the product of the reaction catalyzed by 5-formyltetrahydrofolate cycloligase (EC 6.3.3.2) on 5-FTHF using ATP as a source of chemical energy (Anguera *et al.*, 2003). 5,10-Methenyltetrahydrofolate then enters into the one-carbon metabolic pathway (Stover & Schirch, 1993). 5-FTHF is unique because it does not directly participate as a cofactor in folate-dependant reactions, but acts as an inhibitor of various folate-dependent enzymes (Field *et al.*, 2006). 5-FTHF can regulate folate-dependent one-carbon metabolism by inhibiting folate-dependent enzymes, specifically targeting *de novo* purine biosynthesis. The results of these studies have led to the hypothesis that 5-formyltetrahydrofolate is a chemically stable storage form of folate. In summary, 5-FTHF may function as a source of folates and/or regulate one-carbon metabolism in the pathway shown in Fig. 1 (Ogwang *et al.*, 2011; Stover & Schirch, 1993). The detailed role of the 5-FTHF–EfTS complex in bacterial metabolism will be the subject of future work.

We thank Dr Janet Finer-Moore for helpful discussions and critical reading of the manuscript. We thank Dr Tim Fritz for providing the EfTS clone. We also acknowledge ESRF (Grenoble) for providing access to the ID23.2 beamline. This research was partially funded by Italian MIUR-PRIN 2009 (contract FAKHZT_001) and by Fondazione Cassa di Risparmio di Modena.

References

Anderson, A. C., O'Neil, R. H., DeLano, W. L. & Stroud, R. M. (1999). *Biochemistry*, **38**, 13829–13836.
Anguera, M. C., Suh, J. R., Ghandour, H., Nasrallah, I. M., Selhub, J. & Stover, P. J. (2003). *J. Biol. Chem.* **278**, 29856–29862.
Benvenuti, M. & Mangani, S. (2007). *Nature Protoc.* **2**, 1633–1651.
Berger, S. H., Berger, F. G. & Lebioda, L. (2004). *Biochim. Biophys. Acta*, **1696**, 15–22.
Birdsall, B., Burgen, A. S., Hyde, E. I., Roberts, G. C. & Feeney, J. (1981). *Biochemistry*, **20**, 7186–7195.
Birdsall, D. L., Finer-Moore, J. & Stroud, R. M. (2003). *Protein Eng.* **16**, 229–240.
Carreras, C. W. & Santi, D. V. (1995). *Annu. Rev. Biochem.* **64**, 721–762.
Chu, E., Callender, M. A., Farrell, M. P. & Schmitz, J. C. (2003). *Cancer Chemother. Pharmacol.* **52**, S80–S89.
Costi, M. P., Gelain, A., Barlocco, D., Ghelli, S., Soragni, F., Reniero, F., Rossi, T., Ruberto, A., Guillou, C., Cavazzuti, A., Casolari, C. & Ferrari, S. (2006). *J. Med. Chem.* **49**, 5958–5968.
Costi, P. M., Rinaldi, M., Tondi, D., Pecorari, P., Barlocco, D., Ghelli, S., Stroud, R. M., Santi, D. V., Stout, T. J., Musiu, C., Marangiu, E. M., Pani, A., Congiu, D., Loi, G. A. & La Colla, P. (1999). *J. Med. Chem.* **42**, 2112–2124.
Deshpande, L. M., Fritsche, T. R., Moet, G. J., Biedenbach, D. J. & Jones, R. N. (2007). *Diagn. Microbiol. Infect. Dis.* **58**, 163–170.
Emsley, P. & Cowtan, K. (2004). *Acta Cryst.* D**60**, 2126–2132.
Evans, P. (2006). *Acta Cryst.* D**62**, 72–82.
Ferrari, S., Costi, P. M. & Wade, R. C. (2003). *Chem. Biol.* **10**, 1183–1193.
Field, M. S., Szebenyi, D. M. & Stover, P. J. (2006). *J. Biol. Chem.* **281**, 4215–4221.
Finer-Moore, J. S., Anderson, A. C., O'Neil, R. H., Costi, M. P., Ferrari, S., Krucinski, J. & Stroud, R. M. (2005). *Acta Cryst.* D**61**, 1320–1334.
Finer-Moore, J. S., Fauman, E. B., Foster, P. G., Perry, K. M., Santi, D. V. & Stroud, R. M. (1993). *J. Mol. Biol.* **232**, 1101–1116.
Finer-Moore, J. S., Maley, G. F., Maley, F., Montfort, W. R. & Stroud, R. M. (1994). *Biochemistry*, **33**, 15459–15468.
Fox, K. M., Maley, F., Garibian, A., Changchien, L. M. & Van Roey, P. (1999). *Protein Sci.* **8**, 538–544.
Gibson, L. M., Celeste, L. R., Lovelace, L. L. & Lebioda, L. (2011). *Acta Cryst.* D**67**, 60–66.
Gibson, L. M., Lovelace, L. L. & Lebioda, L. (2008). *Biochemistry*, **47**, 4636–4643.
Gómez-Gil, R., Romero-Gómez, M. P., García-Arias, A., Ubeda, M. G., Busselo, M. S., Cisterna, R., Gutiérrez-Altés, A. & Mingorance, J. (2009). *Diagn. Microbiol. Infect. Dis.* **65**, 175–179.
Hardy, L. W., Finer-Moore, J. S., Montfort, W. R., Jones, M. O., Santi, D. V. & Stroud, R. M. (1987). *Science*, **235**, 448–455.
Hyatt, D. C., Maley, F. & Montfort, W. R. (1997). *Biochemistry*, **36**, 4585–4594.
Krissinel, E. & Henrick, K. (2007). *J. Mol. Biol.* **372**, 774–797.
Laskowski, R. A., MacArthur, M. W., Moss, D. S. & Thornton, J. M. (1993). *J. Appl. Cryst.* **26**, 283–291.
Lee, H., Reyes, V. M. & Kraut, J. (1996). *Biochemistry*, **35**, 7012–7020.
Leslie, A. G. W. (2006). *Acta Cryst.* D**62**, 48–57.
Maley, F., Pedersen-Lane, J. & Changchien, L. (1995). *Biochemistry*, **34**, 1469–1474.
Maley, G. F. & Maley, F. (1988). *J. Biol. Chem.* **263**, 7620–7627.
Mangani, S., Cancian, L., Leone, R., Pozzi, C., Lazzari, S., Luciani, R., Ferrari, S. & Costi, M. P. (2011). *J. Med. Chem.* **54**, 5454–5467.
Matthews, D. A., Appelt, K., Oatley, S. J. & Xuong, N. H. (1990). *J. Mol. Biol.* **214**, 923–936.
Matthews, D. A., Villafranca, J. E., Janson, C. A., Smith, W. W., Welsh, K. & Freer, S. (1990). *J. Mol. Biol.* **214**, 937–948.
Morris, R. J., Perrakis, A. & Lamzin, V. S. (2003). *Methods Enzymol.* **374**, 229–244.
Murshudov, G. N., Skubák, P., Lebedev, A. A., Pannu, N. S., Steiner, R. A., Nicholls, R. A., Winn, M. D., Long, F. & Vagin, A. A. (2011). *Acta Cryst.* D**67**, 355–367.

Ogwang, S., Nguyen, H. T., Sherman, M., Bajaksouzian, S., Jacobs, M. R., Boom, W. H., Zhang, G.-F. & Nguyen, L. (2011). *J. Biol. Chem.* **286**, 15377–15390.
Painter, J. & Merritt, E. A. (2006*a*). *Acta Cryst.* D**62**, 439–450.
Painter, J. & Merritt, E. A. (2006*b*). *J. Appl. Cryst.* **39**, 109–111.
Perry, K. M., Carreras, C. W., Chang, L. C., Santi, D. V. & Stroud, R. M. (1993). *Biochemistry*, **32**, 7116–7125.
Perry, K. M., Fauman, E. B., Finer-Moore, J. S., Montfort, W. R., Maley, G. F., Maley, F. & Stroud, R. M. (1990). *Proteins*, **8**, 315–333.
Pogolotti, A. L., Danenberg, P. V. & Santi, D. V. (1986). *J. Med. Chem.* **29**, 478–482.
Potterton, E., McNicholas, S., Krissinel, E., Cowtan, K. & Noble, M. (2002). *Acta Cryst.* D**58**, 1955–1957.
Sage, C. R., Rutenber, E. E., Stout, T. J. & Stroud, R. M. (1996). *Biochemistry*, **35**, 16270–16281.
Schiffer, C. A., Clifton, I. J., Davisson, V. J., Santi, D. V. & Stroud, R. M. (1995). *Biochemistry*, **34**, 16279–16287.
Segel, I. H. (1975). *Enzyme Kinetics. Behaviour and Analysis of Rapid Equilibrium and Steady-state Enzyme Systems.* New York: John Wiley & Sons.
Spencer, H. T., Villafranca, J. E. & Appleman, J. R. (1997). *Biochemistry*, **36**, 4212–4222.
Stout, T. J., Tondi, D., Rinaldi, M., Barlocco, D., Pecorari, P., Santi, D. V., Kuntz, I. D., Stroud, R. M., Shoichet, B. K. & Costi, M. P. (1999). *Biochemistry* **38**, 1607–1617.
Stover, P. & Schirch, V. (1993). *Trends Biochem. Sci.* **18**, 102–106.
Teuber, M., Schwarz, F. & Perreten, V. (2003). *Int. J. Food Microbiol.* **88**, 325–329.
Vagin, A. & Teplyakov, A. (2010). *Acta Cryst.* D**66**, 22–25.
Winn, M. D. *et al.* (2011). *Acta Cryst.* D**67**, 235–242.
Winn, M. D., Isupov, M. N. & Murshudov, G. N. (2001). *Acta Cryst.* D**57**, 122–133.